STABILITY OF PHASE SPACE DISTRIBUTIONS IN TWO DIMENSIONAL BEAMS

Robert L. Gluckstern*
University of Massachusetts, Amherst

Renate Chasman
Brookhaven National Laboratory

Kenneth Crandall
Los Alamos Scientific Laboratory

ABSTRACT

The most convenient method for including space charge forces in beam dynamics calculations is that proposed by Kapchinsky and Vladimirsky. This distribution corresponds to an ellipsoidal shell in 4-dimensional phase space, leading to uniform distributions in all two dimensional projections, and to linear space charge forces. Beam emittance measurements are for the most part not completely consistent with the KV distribution. Phase space and real space projections indicate instead a central core of high density surrounded by a tail or halo of lower density. The present work is an effort to determine whether or not the matched KV distribution is stable. Numerical orbit calculations for an azimuthally symmetric unaccelerated KV beam have been performed with a constant externally applied radial restoring force in an effort to see whether the distribution in the total energy of each particle remains unchanged. In addition, a family of other stationary 4-dimensional phase space distributions is studied analytically and computationally. The total beam energy for fixed intensity and rms emittance is explored in an effort to determine which distribution is most stable.

I. Introduction

Calculations have recently been performed[1] to study the motion of a Kapchinsky-Vladimirsky (KV) two dimensional beam,[2] including space charge forces. These calculations in some cases lead to a change in distribution, suggesting that some distribution other than the KV one may be more stable. In order to study this question we have evaluated the total energy in beams of different distribution, for the same beam intensity and rms projected phase space area.

In the present work, we shall consider a phase space distribution which is a power law in the total energy.[3] This case includes the KV distribution. A more complete discussion, including long tail distributions, is included in a BNL Report by the present authors.[4]

II. General Formulation

The equation of motion in the transverse direction will be taken to be

$$\ddot{x} + kx = -\frac{e}{m}\frac{x}{r}\frac{d\phi}{dr}$$
$$\ddot{y} + ky = -\frac{e}{m}\frac{y}{r}\frac{d\phi}{dr} \qquad (1)$$

where $-m\vec{kr}$ is the linear external restoring force and $\phi(r)$ is the electrostatic potential due to the space charge of the beam. The energy integral is

$$W = \frac{\sigma^2}{2} + G(r) \qquad (2)$$

where

$$\sigma^2 = u^2 + v^2 \ , \ u = \dot{x}, \ v = \dot{y}, \quad G(r) = \frac{kr^2}{2} + \frac{e}{m}\phi(r) \qquad (3)$$

We can insure a stationary phase space distribution $f(x,y,u,v)$ by constraining f to depend only on W. In this case, one has for the charge density

$$\rho(r) = e\iint du\, dv\, f(W) = \pi e \int_o^\infty d\sigma^2 f(\frac{\sigma^2}{2} + G(r)) \ . \qquad (4)$$

Since the potential ϕ satisfies the Poisson equation, one finds, from (3)

$$\frac{1}{r}\frac{d}{dr}(r\frac{dG}{dr}) = 2k - \frac{\pi e^2}{m\varepsilon}\int_o^\infty d\sigma^2 f(\frac{\sigma^2}{2} + G) \qquad (5)$$

Equation (5) must be solved for $G(r)$ for each choice of distribution function $f(W)$. The number of particles per unit length, N, is then

$$N = \pi^2 \int_o^\infty dr^2 \int_o^\infty d\sigma^2 f(\frac{\sigma^2}{2} + G(r)) = \frac{\pi}{e}\int_o^\infty dr^2 \rho(r) \ . \qquad (6)$$

The total energy U_T is made up of a kinetic energy U_k, the potential energy in the external field U_{ext}, and the electrostatic energy U_{el}. These are given by

$$U_k = \frac{m\pi^2}{2}\int_o^\infty dr^2 \int_o^\infty \sigma^2 d\sigma^2 f(\frac{\sigma^2}{2} + G(r)) \qquad (7)$$

$$U_{ext} = \frac{mk\pi}{2e}\int_o^\infty r^2 dr^2 \rho(r) \qquad (8)$$

$$U_{el} = -\frac{1}{2\varepsilon}\int_o^\infty dr^2 \rho(r) Q(r) \ln\frac{r}{r_o} \qquad (9)$$

where r_o is the radius of a large cylinder at which the potential is taken to vanish and $Q(r)$ is the charge within the radius r, i.e.,

$$Q(r) = \pi\int_o^{r^2} dr^2 \rho(r) \ , \quad Q'(r) = 2\pi r\rho(r) \ . \qquad (10)$$

Finally, the rms area of the $(x\text{-}x')$ phase space projection can be taken to be

$$\left(\frac{2A_x}{\pi}\right)^2 = 4\,\overline{x^2}\ \overline{\dot{x}^2} = \overline{r^2}\ \overline{\sigma^2} = \frac{2}{mk}\frac{U_{ext}}{N} \cdot \frac{2}{m}\frac{U_k}{N} \qquad (11)$$

We shall find it convenient to express our results in terms of the three dimen-

sionless parameters

$$\mu = \frac{e\rho(o)}{2m\epsilon k} \qquad \text{(ratio of electrostatic repulsion to restoring force at beam center)} \tag{12}$$

$$p = \frac{4m\epsilon\sqrt{k}}{\epsilon^2} \cdot \frac{A_x}{N} \qquad \text{(emittance per particle)} \tag{13}$$

$$q = \frac{4\pi\epsilon}{e^2} \cdot \frac{U_T}{N^2} \qquad \text{(energy divided by the square of the beam intensity)} \tag{14}$$

In terms of the energies, one has, from (11),

$$p = \frac{4\pi\epsilon}{e^2} \cdot \frac{\sqrt{U_{ext} U_k}}{N^2} \tag{15}$$

III. Power Law Distribution[5]

Let us take for a distribution in phase space

$$f(W) = nB(W_o - W)^{n-1} \tag{16}$$

where the factor n is introduced to allow us to interpret the n = o limit, which turns out to be equivalent to the KV distribution. From (4) one finds

$$\rho(r) = \begin{cases} 2\pi eB(W_o - G)^n & G(r) < W_o \\ o & G(r) > W_o \end{cases} \tag{17}$$

and from (12)

$$\mu = \frac{\pi e^2 B}{m\epsilon k} (W_o - G_o)^n \tag{18}$$

The function G(r) is determined from (6). Using the dimensionless parameter

$$g(r) = \frac{W_o - G(r)}{W_o - G_o} \quad , \quad R = \sqrt{\frac{2k}{W_o - G_o}}\ r \tag{19}$$

one obtains the equation

$$\frac{1}{R}\frac{d}{dR}\left(R \frac{dg}{dR}\right) = -1 + \mu g^n \quad , \ g(0) = 1, \ g'(0) = 0 \quad . \tag{20}$$

Equation (20) can be solved for a particular value of μ, and the "border" of the charge distribution is the radius at which g vanishes. Once g is obtained, the evaluation of energies and phase space areas is a straightforward matter. From (17) one has for the charge density and number of particles per unit length,

$$\rho(r) = 2\pi eB(W_o - G_o)^n\ g^n \tag{21}$$

and

$$N = \frac{\pi^2 B}{k} (W_o - G_o)^{n+1} \int_o^\infty dR^2\ g^n \tag{22}$$

where the integral is taken to the border of the charge distribution. The quantity Q(r) is obtained from (10)

$$Q(r) = \frac{\pi^2 eB}{k} (W_o - G_o)^{n+1} \int_o^{R^2} dR^2 \; g^n \tag{23}$$

The energies are found from (7), (8), (9) to be

$$U_k = \frac{m\pi^2 B(W_o - G_o)^{n+2}}{k(n+1)} \int_o^{\infty} dR^2 \; g^{n+1} \tag{24}$$

$$U_{ext} = \frac{m\pi^2 B(W_o - G_o)^{n+2}}{4k} \int_o^{\infty} R^2 dR^2 \; g^n \tag{25}$$

$$U_{el} = -\frac{\mu_B m\pi^2 B(W_o - G_o)^{n+2}}{4k} \int_o^{\infty} dR^2 \; g^n \ln R^2 \int_o^{R^2} dR^2 \; g^n \tag{26}$$

$$- \frac{e^2}{8\pi\epsilon} N^2 \ln \frac{W_o - G_o}{2r_o^2 k} \quad ,$$

leading finally to the parameters

$$p = \frac{2}{\mu\sqrt{n+1}} \cdot \frac{\left[\int_o^{\infty} dR^2 g^{n+1} \int_o^{\infty} dR^2 g^n R^2\right]^{1/2}}{\left[\int_o^{\infty} dR^2 g^n\right]^2} \tag{27}$$

$$q - q_o = \frac{\frac{1}{\mu}\left[\frac{4}{n+1}\int_o^{\infty} dR^2 g^{n+1} + \int_o^{\infty} dR^2 g^n R^2\right] - \int_o^{\infty} dR^2 g^n \ln R^2 \int_o^{R^2} dR^2 g^n}{\left[\int_o^{\infty} dR^2 g^n\right]^2} + \frac{\ell n(\mu \int_o^{\infty} dr^2 g^n}{2} \tag{28}$$

where

$$2q_o = \ell n(2\pi m\epsilon k r_o^2 / Ne^2)$$

Equations (27) and (28) together with (20) give p and q in terms of μ, and hence, q in terms of p. This enables us to examine the total energy of different stationary configurations for different projected phase space area. It can be easily verified[4] that (27) and (28) reduce to the results for the KV distribution when n = 0.

IV. Limiting Values

A. Low Space Charge

In the limit of low space charge, μ tends to zero, p tends to infinity, and g approaches the limit

$$g \tilde{=} 1 - \frac{R^2}{4} \tag{29}$$

It can be readily shown that the kinetic and (external) potential energies are equal in this limit (virial theorem). It is therefore simple to approximate (28) for low μ by replacing the sum in the bracket in the numerator by twice the geometric mean of the two terms, thus preserving the validity of the expression to the lowest two

orders in μ. This leads to

$$p \overset{\sim}{=} \frac{(n+1)}{\mu(n+2)} \quad , \qquad \mu \to 0 \tag{30}$$

$$q \overset{\sim}{=} 2p - \frac{1}{2} \ln p + \alpha_n + q_o \quad , \qquad p \to \infty \tag{31}$$

where

$$\alpha_n = \frac{\Gamma'(n+2)}{\Gamma(n+2)} - \frac{\Gamma'(1)}{\Gamma(1)} - \frac{1}{2}\left(\frac{\Gamma'(2n+3)}{\Gamma(2n+3)} - \frac{\Gamma'(1)}{\Gamma(1)}\right) - \frac{1}{2}\ln(n+2) \tag{32}$$

Table I contains the values of α_n for various n.

Table I

Parameters in Energy Comparison

n	0	1	2	3	4	5	∞
α_n	-.097	-.091	-.085	-.080	-.077	-.075	-.058

It is clear from Table I that in the low space charge limit one finds that the total energy increases as one proceeds from the KV configuration to the power law with increasing n. In fact, one finds from (32) that $\alpha_{-1} = 0$ and $\frac{d\alpha}{dn} = 0$ at n = 0, thus implying (at least for low space charge) that the KV distribution has the lowest energy when compared with power law distributions for both integral and non-integral n. In addition, one can show, for low space charge, that the KV distribution gives a local minimum in energy (q) when compared with neighboring distribution functions, f(W), of arbitrary shape.

B. High Space Charge Limit

In the limit of high space charge, μ approaches 1 and the distributions all tned to uniform density with a relatively sharp surface. In this case one finds

$$q \overset{\sim}{=} \frac{3}{4} + 2p^2 \quad , \qquad p \to 0 \tag{33}$$

independent of n. The second term in (33) results from an analysis which treats (27), (28) in powers of the ratio of the surface "thickness" to the radius of the distribution.

V. Analytic Computations and Discussion

We have obtained covergent series solutions of (20) for g in powers of R^2. The results are shown in Figures 1-4 corresponding to n = 0, 1, 2 and 5, each figure containing curves for several values of the space charge parameter μ. One can readily convert from our dimensionless parameters, g, R^2 to the real radius r, charge density

$\rho(r)$ and electrostatic potential ϕ, by using (17), (18), (19) and (22). Specifically one has

$$\phi(r) = \frac{2m\varepsilon k}{e}\mu g^n \quad , \quad r^2 = R^2 \frac{e^2}{2m\varepsilon k\pi} \cdot \frac{N}{\mu J} \quad , \quad \phi(r) = \frac{Ne}{\pi\varepsilon}\frac{1-g-\frac{R^2}{4}}{\mu J} \tag{34}$$

where

$$J = \int_0^{R_m^2} g^n \, dR^2 \quad , \tag{35}$$

taken to the radius where g vanishes, is the normalizing integral for the charge. Values of J are indicated in the figures.

Figure 5 shows the variation of q with p for n = 0 and n = 5. All the curves from n = 0 to n = ∞ cluster remarkably close together -- so much so that it is difficult to tell from the figure which curve is lowest. In order to compare the different distribution more accurately, we have computed the two parameters $\bar{q}$ and $\bar{p}$ given by

$$\bar{q} = q - 2p + \frac{1}{2}\ell n(\frac{1}{4} + p) - q_o \quad , \quad \bar{p} = (\frac{4p}{1+4p})^2 \quad . \tag{36}$$

We have plotted $\bar{q}$ vs $\bar{p}$ for different n in Figure 6. These results show that $\bar{q}$ (or q) is lowest for fixed $\bar{p}$ (or p) for the KV distribution, although the expanded scale for $\bar{q}$ indicates that the energy difference between distributions is remarkably small.

It is tempting to conclude from Figure 6 that the KV distribution is the "most stable". By this we would mean that a KV distribution would remain unchanged as it drifted, while any other distribution would eventually go into the KV distribution. Unfortunately we are not permitted to draw such a conclusion, since we are here comparing distributions for fixed projected rms phase space area (p), a quantity which is unlikely to remain constant if and when the distribution should change. Moreover, we are here only considering a particular family of distributions in phase space.

Liouville's theorem does not apply directly to phase space projected areas. Furthermore, it applies only to local phase space densities; a rearrangement of these densities can cause either an increase or a decrease in the rms area. In addition, density fluctuations and other non-linear effects usually cause distortions of phase space. These distortions, sometimes in the form of filamentation, keep the two phase space areas invariant but often "capture" regions of "empty" phase space, thus increasing the apparent phase space area. Since space charge forces are related to actual charge densities, they are dependent on the apparent phase space area, which may very well increase.

For these reasons, it may not be correct to compare the energies of different

distributions for the same rms projected area. All that can be said at this point is that we are unable to find a distribution which, for fixed p, provides a value of q below that for n = 0.

VI. Numerical Calculations and Discussion

Various initially self-consistent distributions were followed numerically over large distances in order to see if the statistical fluctuations in the computation could cause a transition between two such distributions.

The computer program[6] which was used for these calculations assumed radial symmetry. This means that the input distributions were radially symmetric and that radial forces only (focussing and space forces) were applied. Space charge forces were calculated using Gauss' law. The integration of the euqations of motion of the individual particles was done in an iterative way which assured conservation of the total energy of the system. This quantity varied by less than 0.2% over 10,000 integration steps. Furthermore, angular momentum of the individual particles was conserved to better than 1 in 10^{+6}.

The distribution N(W) in the energies W (normalized to zero at the center of the beam) of the individual particles was observed along the distance over which the beam was simulated. The connection between this distribution and the phase space distribution f(W), defined earlier in this paper, can easily be seen if all forces are linear. In this case the volume element in phase space, dxdydudv, is proportional to WdW. The number of particles per volume element is therefore proportional to f(W)WdW and N(W) is proportional to Wf(W).

One can characterize the distribution N(W), to lowest order, by its average, W_{av}, by its rms width, ΔW. The ratio $\Delta W/W_{av}$ was used to describe the distribution N(W) through the numerical computation.

It should be pointed out that, in the linear space charge force approximation, $\Delta W/W_{av}$ can easily be calculated theoretically for different forms of f(W). Single integrations give the following results for a few cases:

Table II

f(W)	$\Delta W/W_{av}$
A $\delta(W-W_o)$ (n=0)	0
B (n=1)	$\sqrt{2}/4$
C exp(-W) (n=∞)	$\sqrt{2}/2$

Other quantities such as the rms value of the x-coordinates, the rms x-u phase space area and the radial charge distribution, were also recorded throughout the computations. In all runs the current was chosen to be 200 mA and the emittance was adjusted so that its corresponding rms area was that of a 4.5 π cm-mrad KV beam for $\beta = 0.4$. Runs were made for different numbers of particles, ranging from 250 to 5000.

Computer runs were made for the KV (or n=0) distribution for several different values of the space charge parameter μ defined in (12). This was done by varying the strength of the external restoring force. The input distributions were obtained by populating uniformly very thin hyperellipsoidal shells in four-dimensional phase space.

Figures 7 and 8 show results for $\Delta W/W_{av}$ versus s, the traveling distance of the beam, for $\mu = 0.75$ and $\mu = 0.954$ from runs with 250, 500, 1000 and 2500 particles. The runs extended to 50 m and 105 m for $\mu = 0.75$ and $\mu = 0.954$ respectively. The initial values of $\Delta W/W_{av}$ are different from zero (the theoretical value) in all cases due to fluctuations in the charge density caused by the finite number of particles used in the calculation. For $\mu = 0.75$ a steady growth of $\Delta W/W_{av}$ is seen. The growth rate increases consistently as the number of particles, N, used to simulate the beam, decreases. Quantitatively, the curves in Fig. 7 seem to indicate that $\Delta W/W_{av}$ at a certain distance, s, varies roughly as $N^{-1/2}$. One, therefore can not rule out that the possibility that the growth of $\Delta W/W_{av}$, which shows up in the case of $\mu = 0.75$, may solely be due to the model by which the beam is described in the computer program. (i.e., as a collection of macroparticles). For $\mu = 0.954$, on the other hand, the growth pattern of $\Delta W/W_{av}$ is quite different. Here $\Delta W/W_{av}$, after an initial growth, levels off to values which are fairly close to each other and do not in any obvious way depend on N, the number of particles used in the calculation. Results obtained with 5000 particles (not shown here) are in agreement with these findings. Runs were also made for $\mu = 0.44$ and lead to conclusions similar to those which were reached for $\mu = 0.75$.

Illustrated in Figs. 9 and 10 are runs with 1000 particles that were extended to 500 m for both $\mu = 0.75$ and $\mu = 0.954$. The quantities, $\Delta W/W_{av}$, x_{rms} and the rms x-u area are shown as functions of s. The results for $\Delta W/W_{av}$ are consistent with those obtained from the shorter runs shown in Figs. 7 and 8. The rms value of the x-coordinates shows small oscillations the frequency of which corresponds to that of the

breathing mode of a mismatched KV beam. A slight initial mismatch is caused by the statistical fluctuations due to the finite number of particles used in the program. The breathing oscillations are superimposed on a slower frequency spectrum, the main features of which also show up in the curves for the rms x-u area. Furthermore, there seems to be a decrease of a few percent in the average rms emittance. Similar results for the change in average rms emittance were obtained in most of the other computer runs.

Figures 11 and 12 show the particle distributions in two dimensional phase space at 0 m and 105 m. For $\mu = 0.954$ the input and output distributions differ considerably whereas for $\mu = 0.75$ only very minor changes seem to occur. Figures 13 and 14 show the distributions in W and the radial charge densities at 0 m and 500 m.

Runs were also made for self-consistent distributions other than those of the KV type (n=0). Phase space distributions for n=1 and n=2 were generated using the series expansion of the dimensionless potnetial function g described in Section V of this paper. The external restoring force which was used with these distributions corresponded to $\mu = 0.44$ for a KV beam. The resulting μ-values were $\mu = 0.54$ for n=1 and $\mu = 0.59$ for n=2. (With fixed external focussing force, current and rms emittance μ will increase with n because the radial charge density at the origin grows as n gets larger.)

Figure 15 shows results which were obtained for n=1. Runs were made with 2500 and 500 particles for 15 m and 35 m respectively and $\Delta W/W_{av}$ was plotted against s. The initial values of $\Delta W/W_{av}$ agree well with that calculated theoretically in the linear space charge approximation and listed in Table II. Results from a run with n=2 and 2500 particles are shown in Fig. 16. There are no signs of instability for the n=1 and n=2 distributions. However, because of the higher initial values of $\Delta W/W_{av}$ for these distributions small changes in this parameter would be difficult to observe.

The results from the numerical calculations which have been described here are not inconsistent with the theoretical conclusions which were presented earlier in this paper. Though the only indication for possible instabilities were found for the KV distribution, there is no contradiction of the theoretical finding that this distribution has the lowest energy for a fixed value of p, the dimensionless rms emittance. Computer results show that the parameter p can, in fact, decrease and therefore, as

illustrated in Fig. 5, transitions from a distribution with n = 0 to a distribution with a higher value of n is possible from the point of view of conservation of energy. Further theoretical confirmation for a possible instability of the KV distribution with high values of μ was found in a study of the oscillation modes of such distributions.[7] One azimuthally symmetric mode appears to have an imaginary frequency for $16/17 < \mu < 1$.

VII. Acknowledgment

The authors would like to thank Miss Frances Munkenbeck and Mr. Peter Milonni for helping with the calculations and programming represented by the Figures. In addition, one of the authors (R. L. Gluckstern), would like to thank Dr. Pierre Lapostolle for his helpful comments on an earlier preprint version of this paper.

References

*Supported by the National Science Foundation and the Atomic Energy Commission.

[1] R. Chasman, private communication (1970), K. Crandall, private communication (1970).

[2] P. M. Kapchinsky and V. V. Vladimirsky, Proceedings of the 2nd International Conference on High Energy Accelerators, CERN, Geneva, p. 274 (1959).

[3] P. Lapostolle and B. Lapostolle, CERN Report ISR-300/LI/69-43, November 5, 1969, have considered the oscillations and energy of a beam which has a uniform distribution in 4-dimensional phase space.

[4] BNL Report - to be published.

[5] This distribution includes that used by P. Lapostolle, CERN Report ISR-300/LI/69-19, April 28, 1969 (n=1), and that used by M. Promé, Saclay Report SEFS TD 69/36-IHE, May 21, 1969 (n=∞). See also F. J. Sacherer, CERN Report SI/Int. DL/70-5, June 24, 1970.

[6] Similar programs have been described by K. R. Crandall, Proc. of the 1966 Linear Accelerator Conference, LA-3609, p. 233 (1966) and by P. Tanguy, CERN Internal Report MPS/Int. LIN 69-11 (1969).

[7] R. L. Gluckstern, Proceedings of the NAL Linac Conference, Batavia (1970).

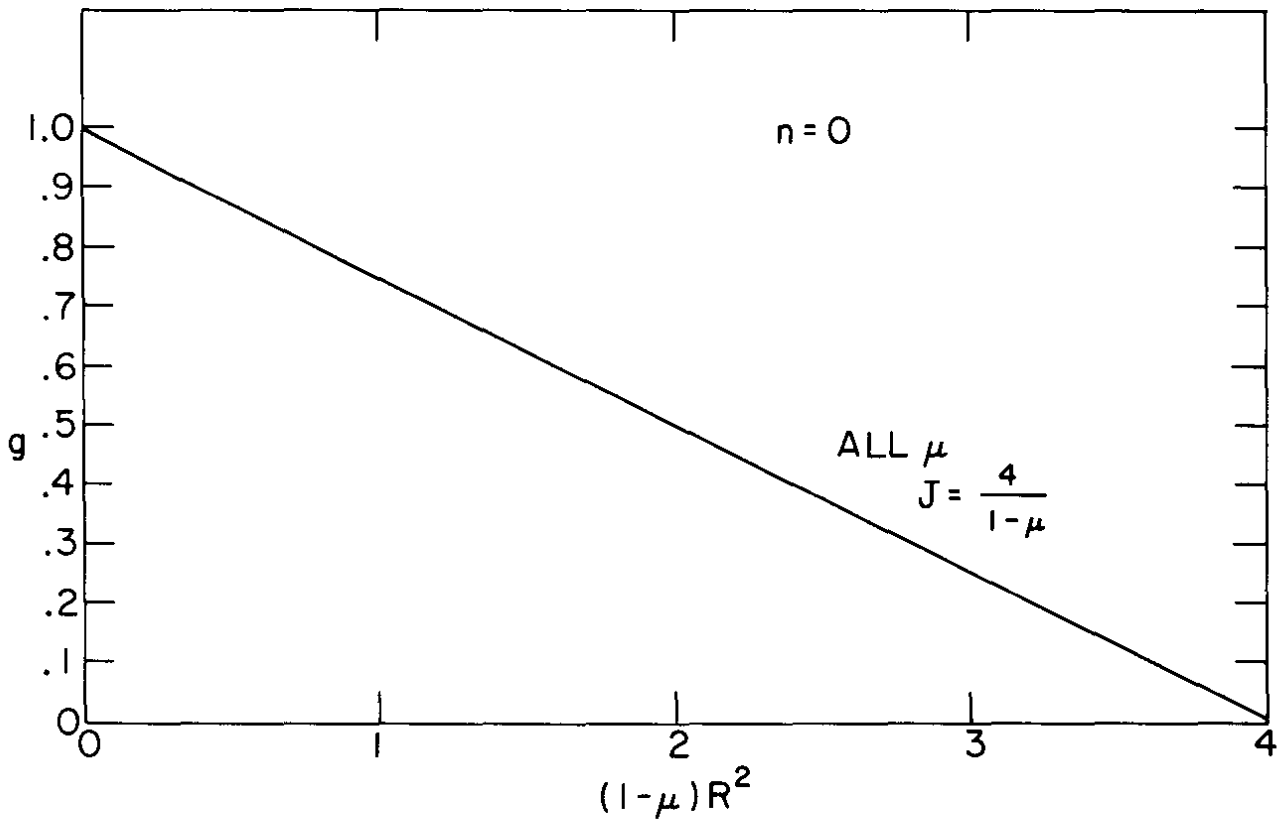

Fig. 1. Dimensionless potential function vs $(1 - \mu)R^2$ for n = 0.

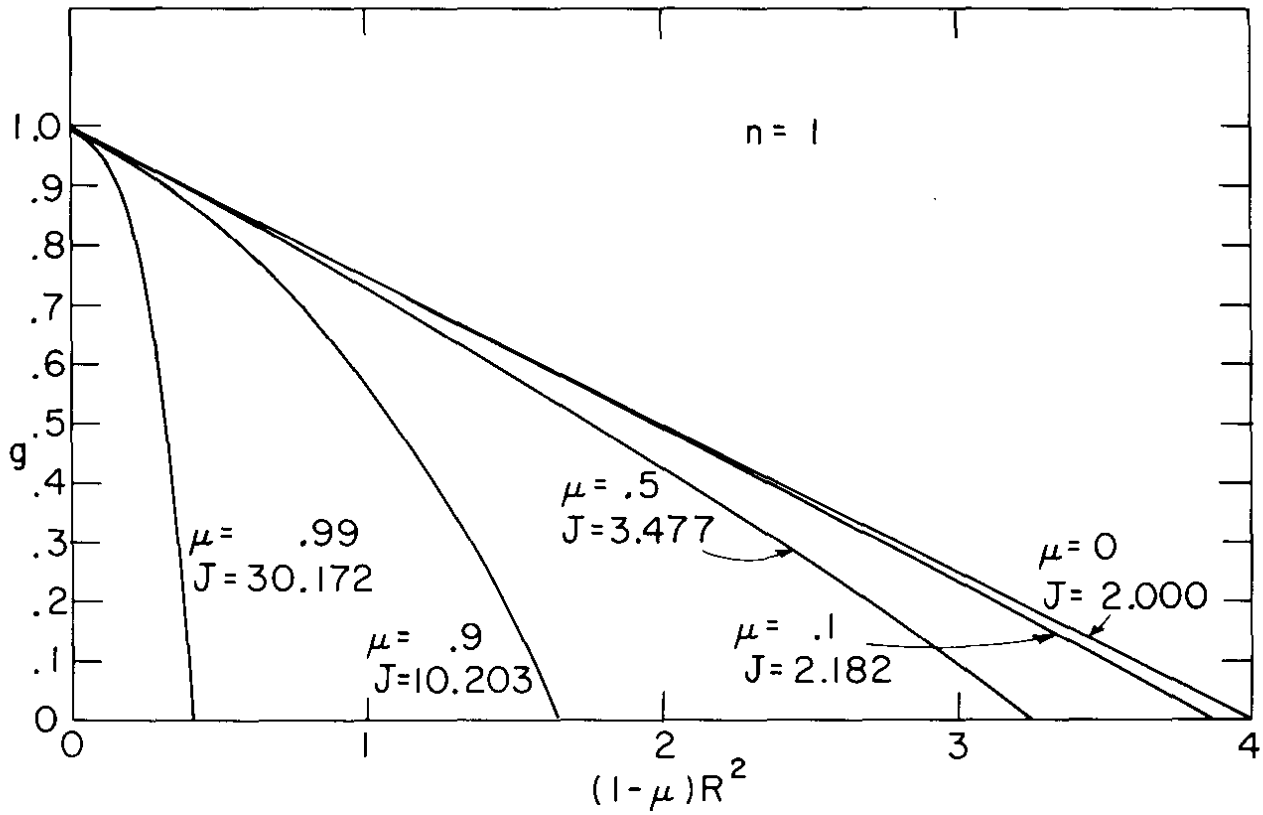

Fig. 2. Dimensionless potential functions vs $(1 - \mu)R^2$ for n = 1.

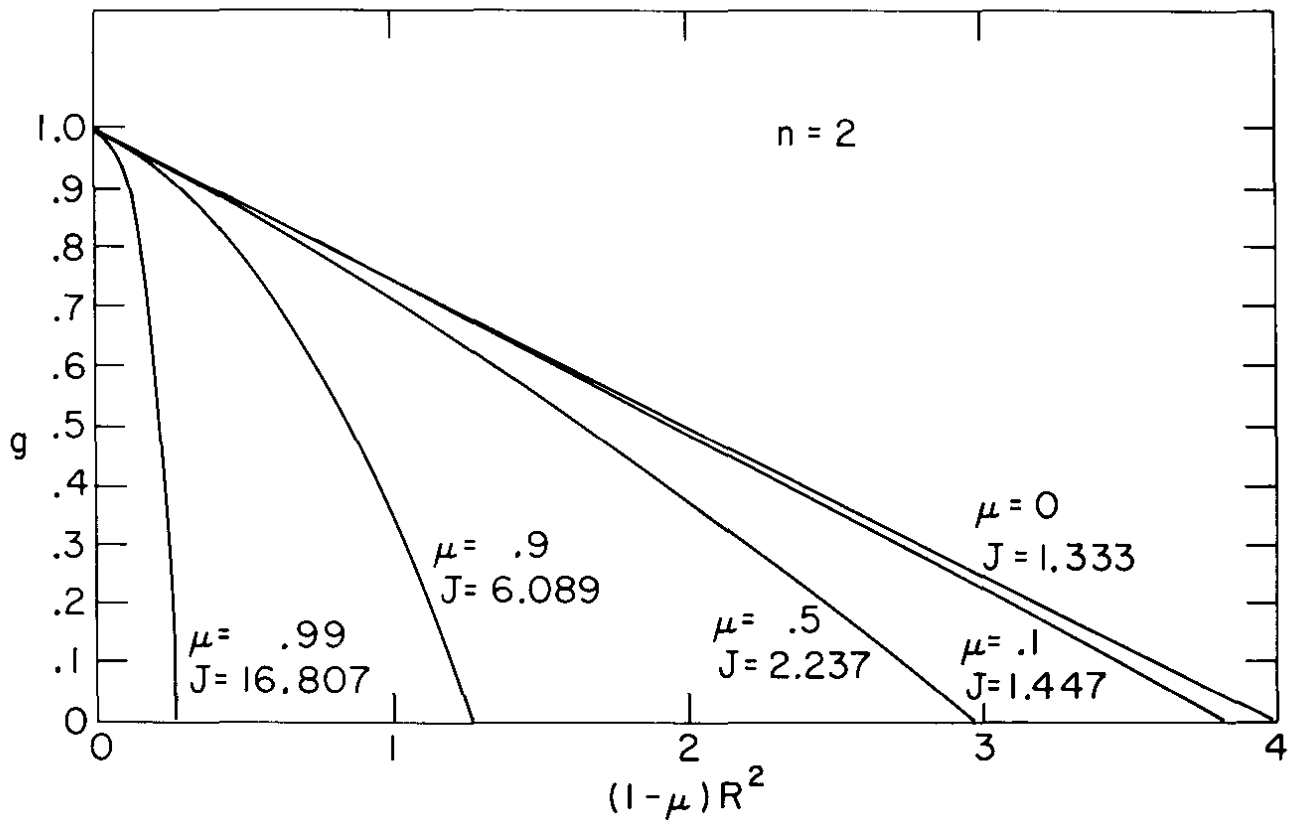

Fig. 3. Dimensionless potential functions vs $(1 - \mu)R^2$ for n = 2.

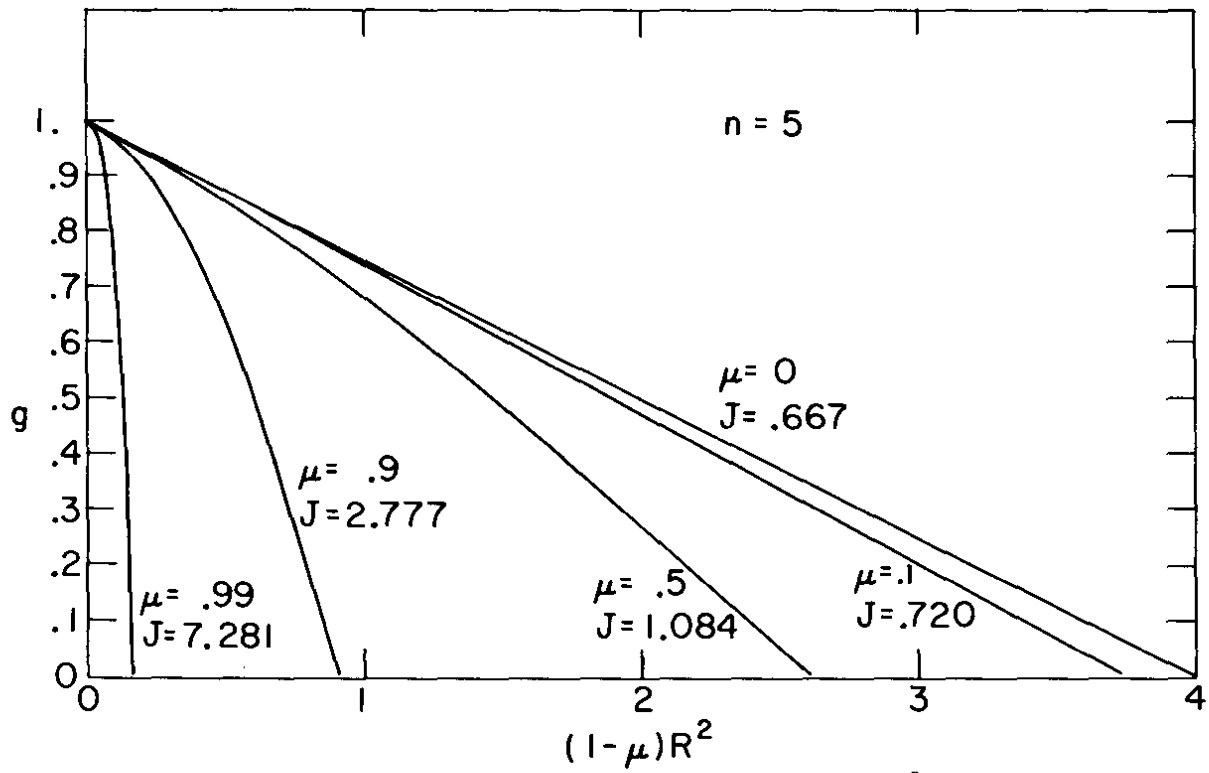

Fig. 4. Dimensionless potential functions vs $(1 - \mu)R^2$ for n = 5.

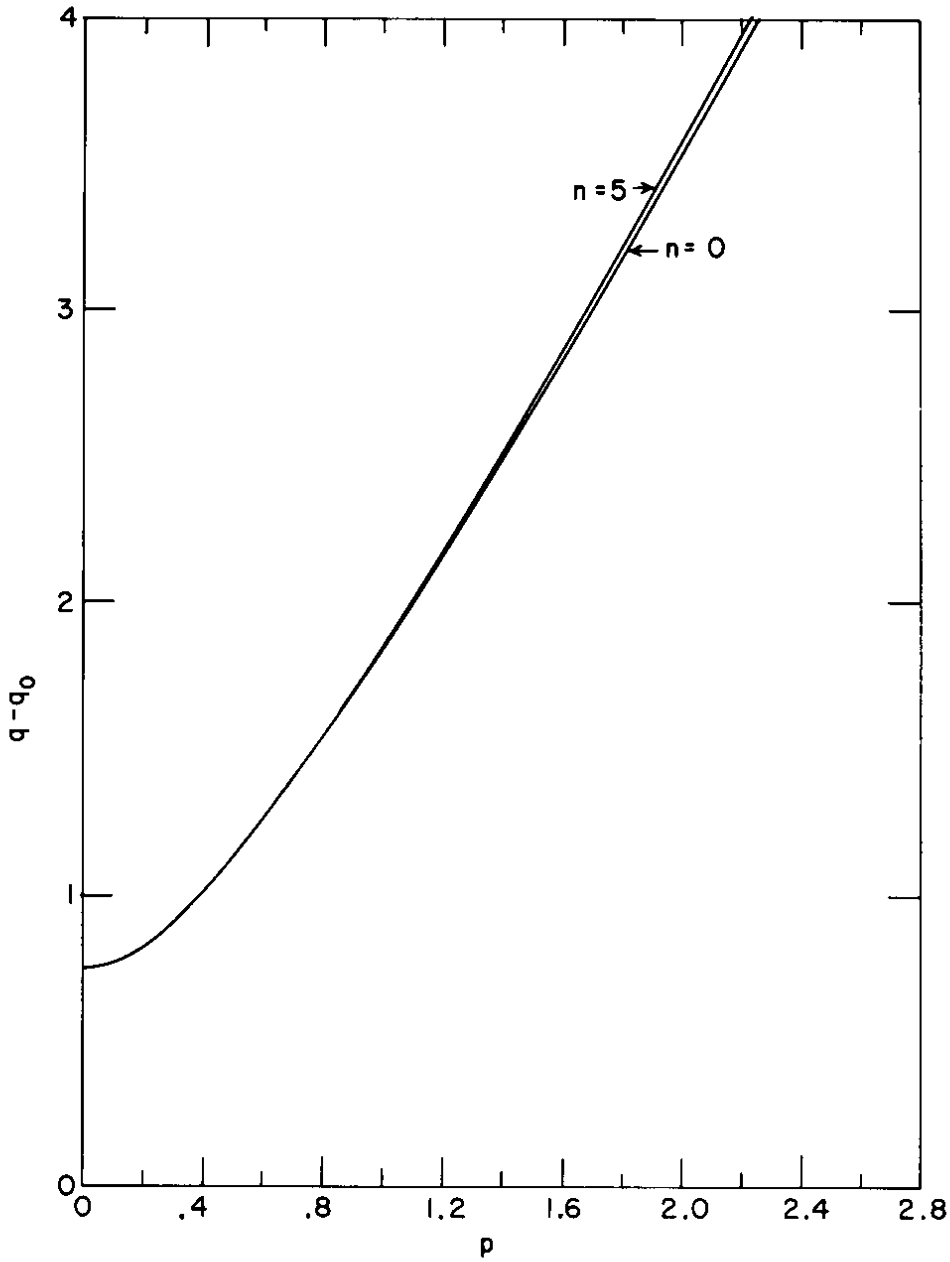

Fig. 5. Energy parameter vs emittance parameter.

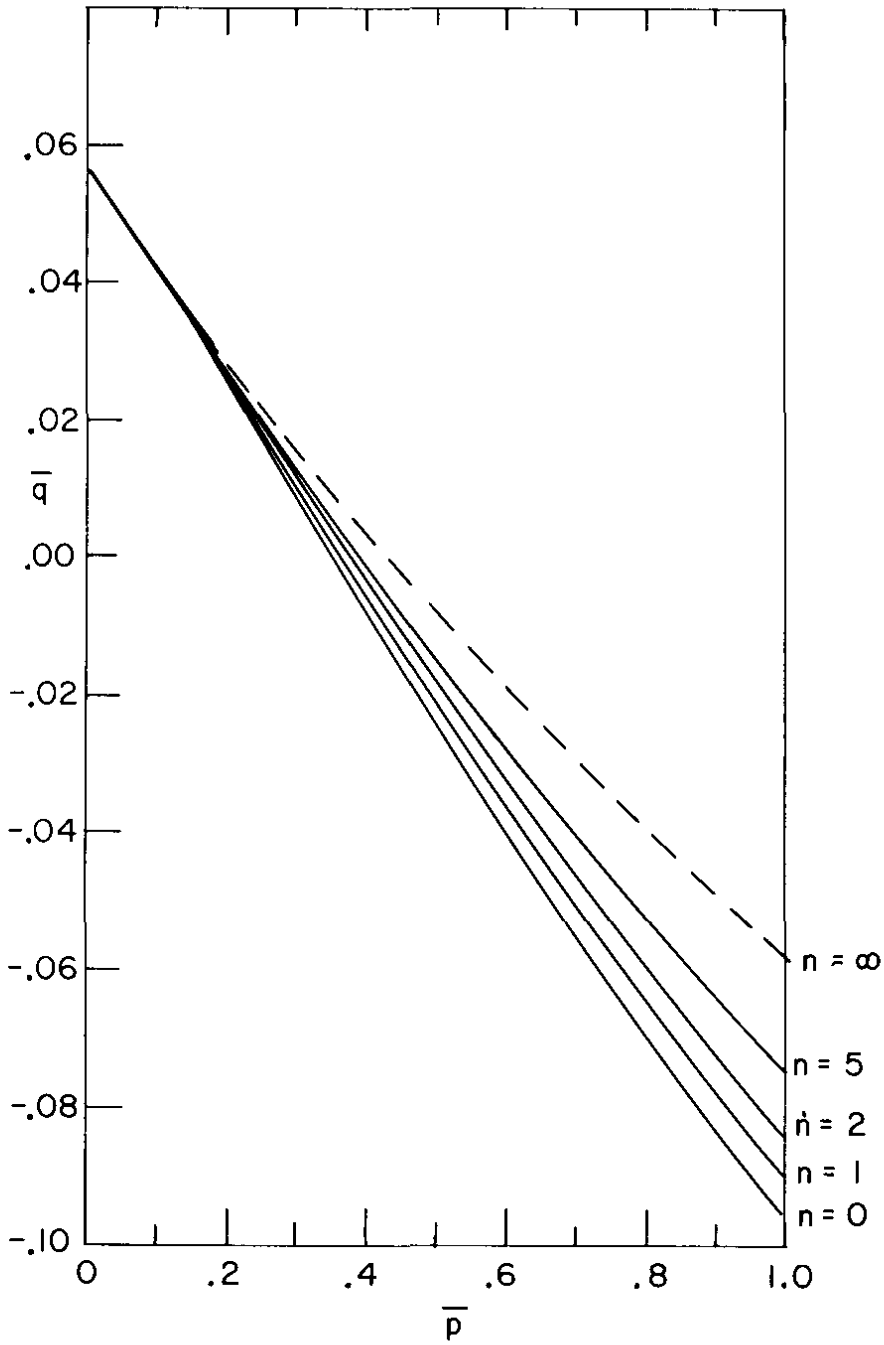

Fig. 6. Modified energy parameter vs emittance parameter.

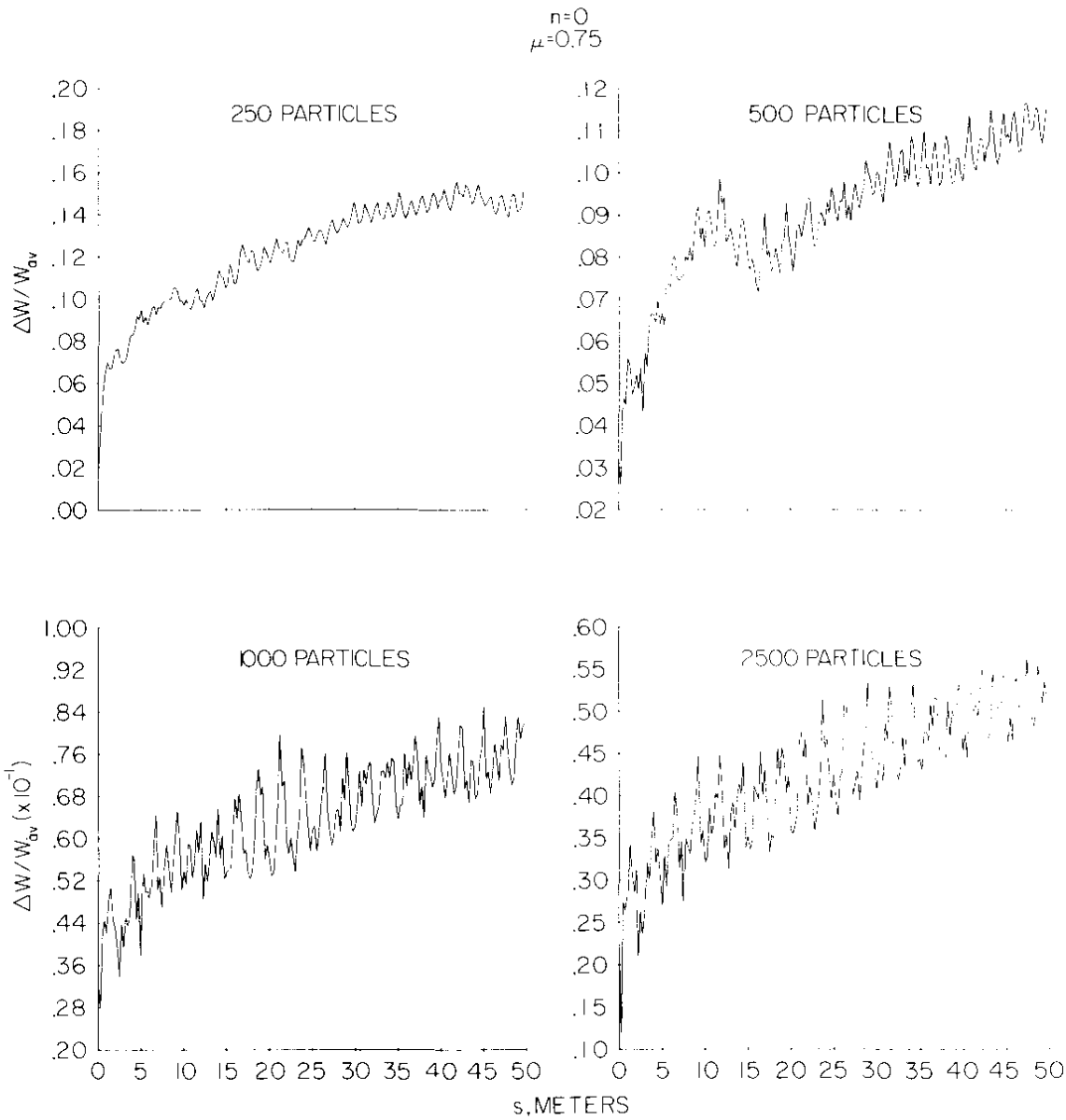

Fig. 7. $\Delta W/W_{av}$ as function of s, for n = 0 and μ = 0.75, obtained from runs with 250, 500, 1000, and 2500 particles.

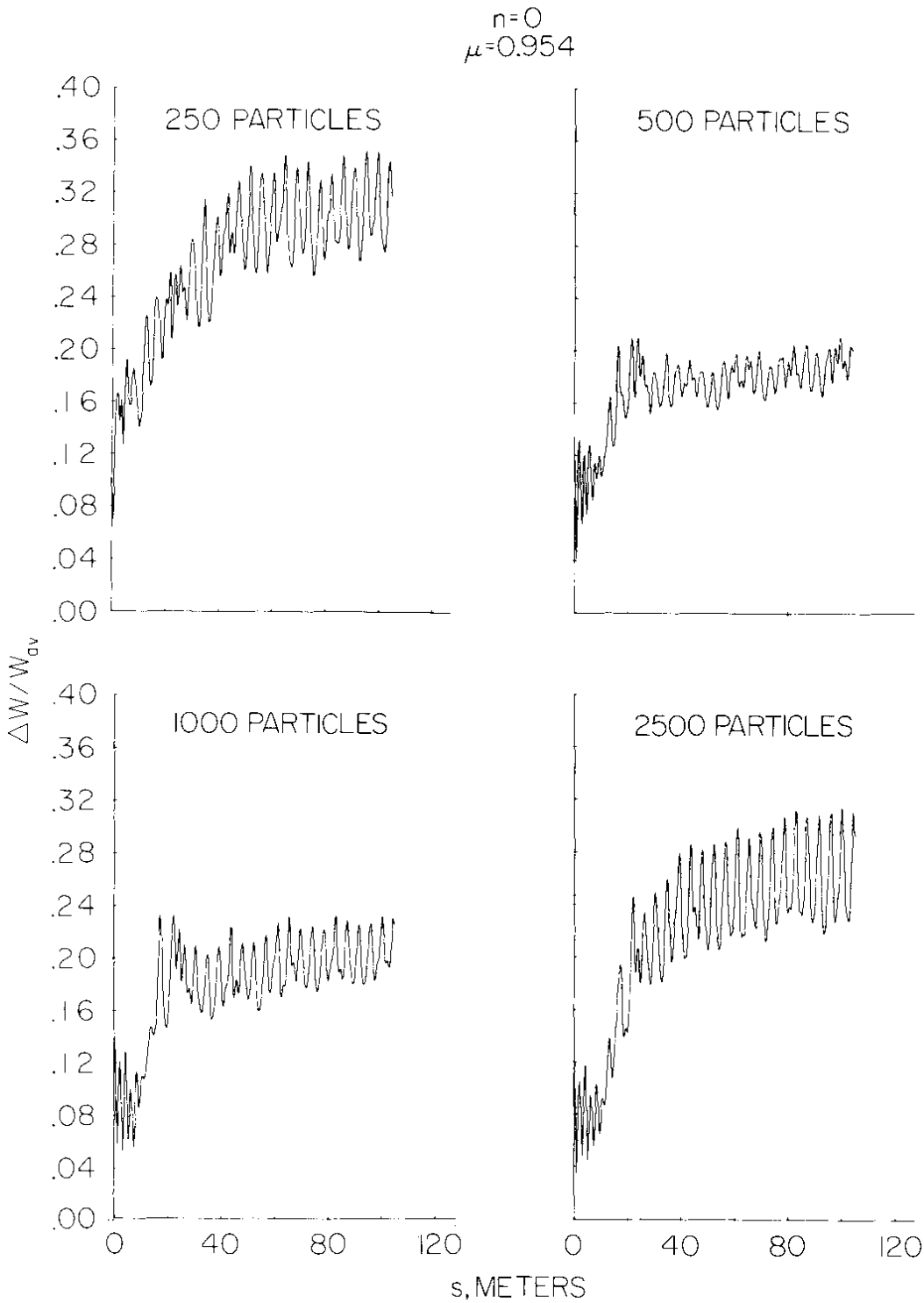

Fig. 8. $\Delta W/W_{av}$ as functions of s, for n = 0 and μ = 0.954, obtained from runs with 250, 500, 1000, and 2500 particles.

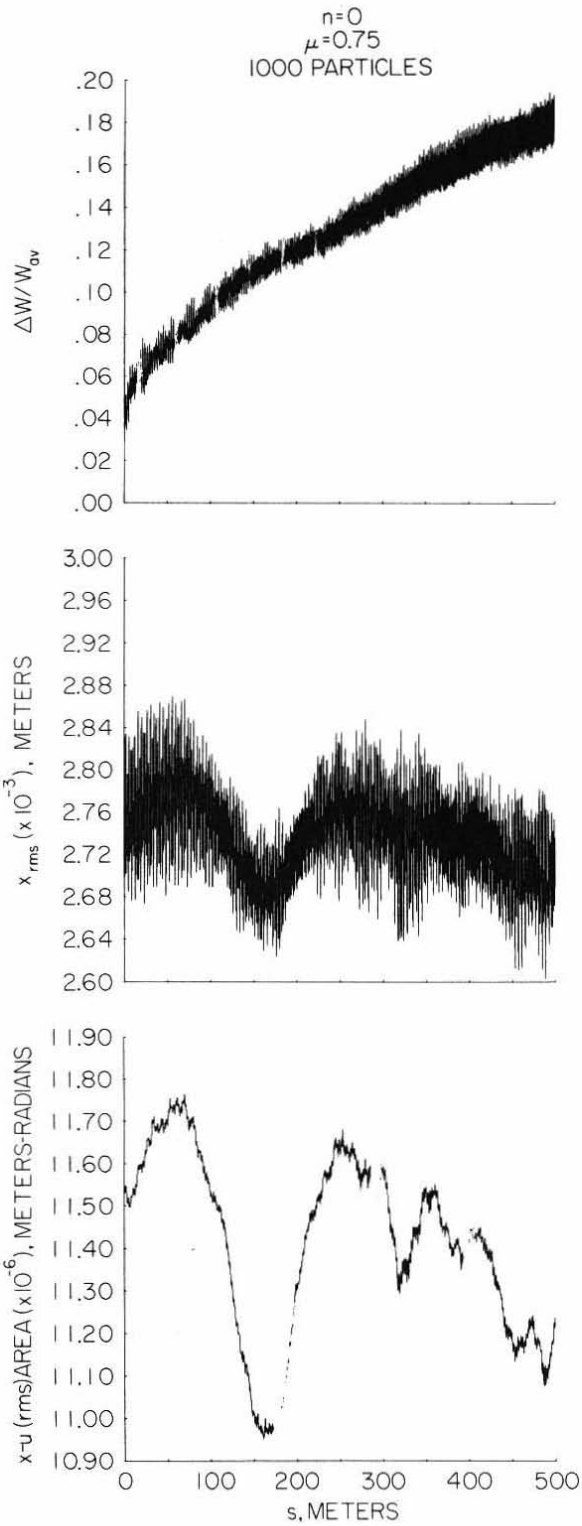

Fig. 9. $\Delta W/W_{av}$, x_{rms} and rms x - u area as functions of s, for n = 0 and μ = 0.75, obtained from run with 1000 particles.

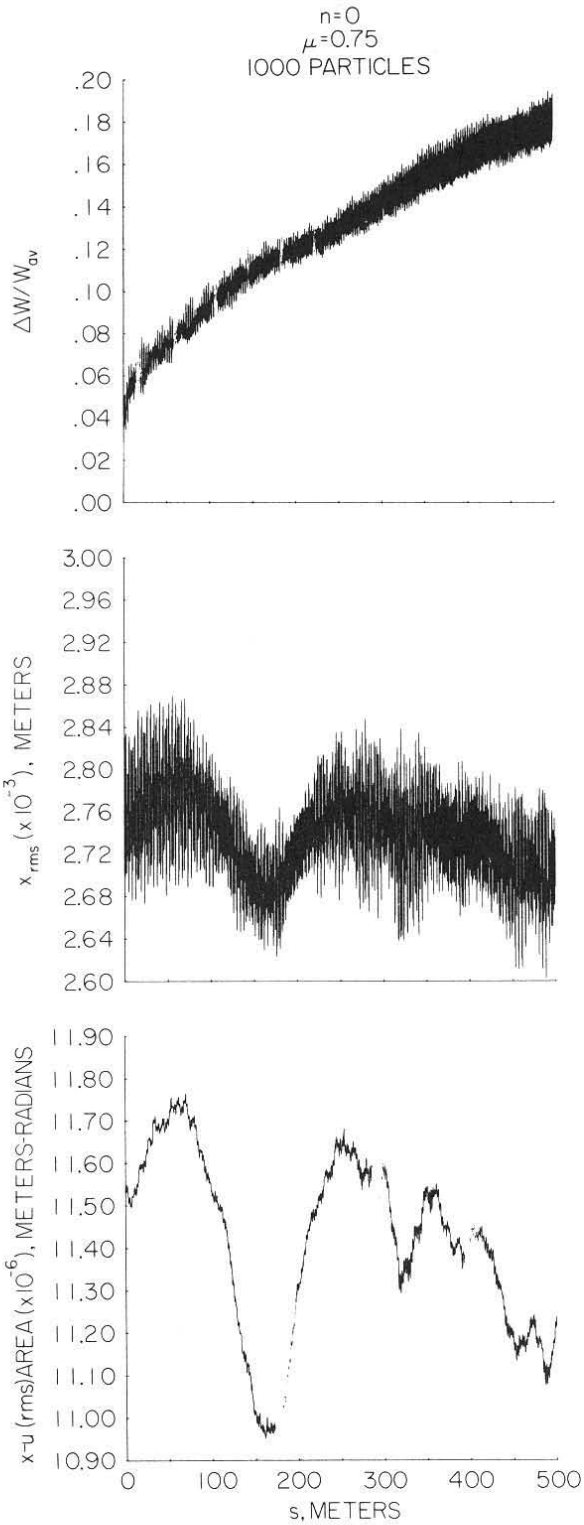

Fig. 9. $\Delta W/W_{av}$, x_{rms} and rms x - u area as functions of s, for n = 0 and μ = 0.75, obtained from run with 1000 particles.

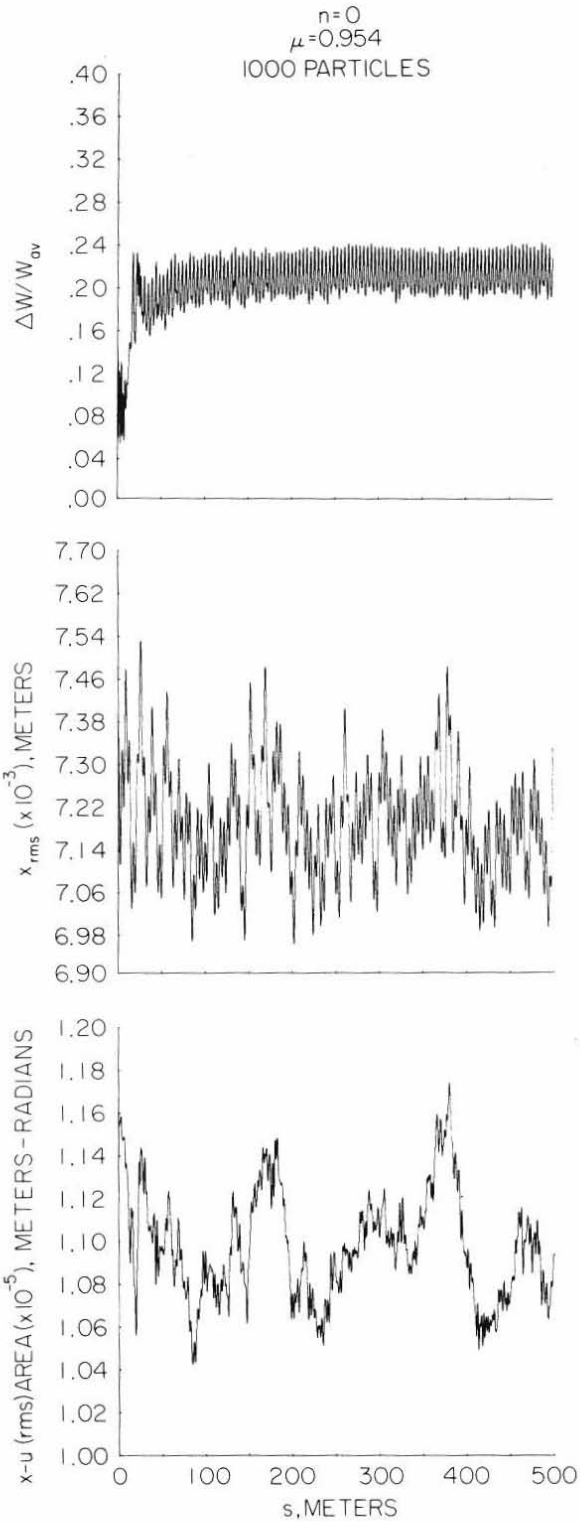

Fig. 10. $\Delta W/W_{av}$, x_{rms} and rms x - u area as functions of s, for n = 0 and μ = 0.954, obtained from run with 1000 particles.

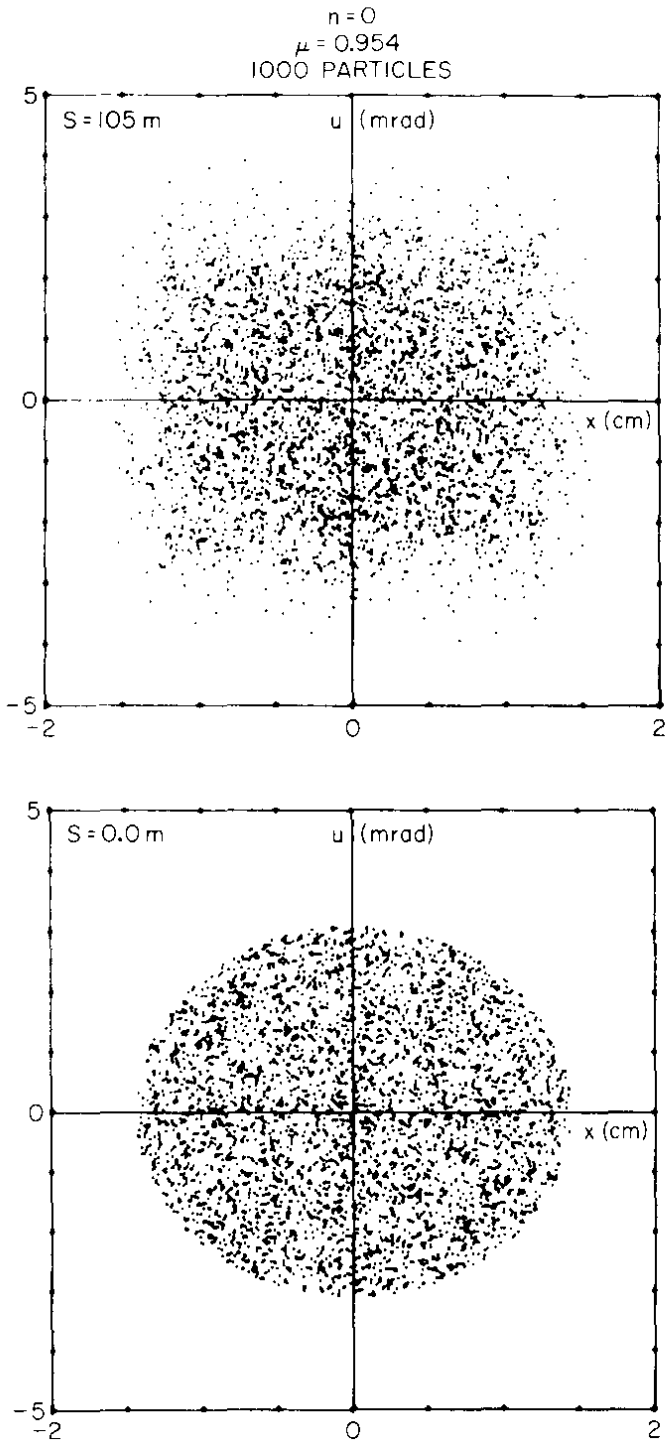

Fig. 12. Particle distribution in two-dimensional phase space at 0 amd 105 m for n = 0 and μ = 0.954, obtained from run with 1000 particles.

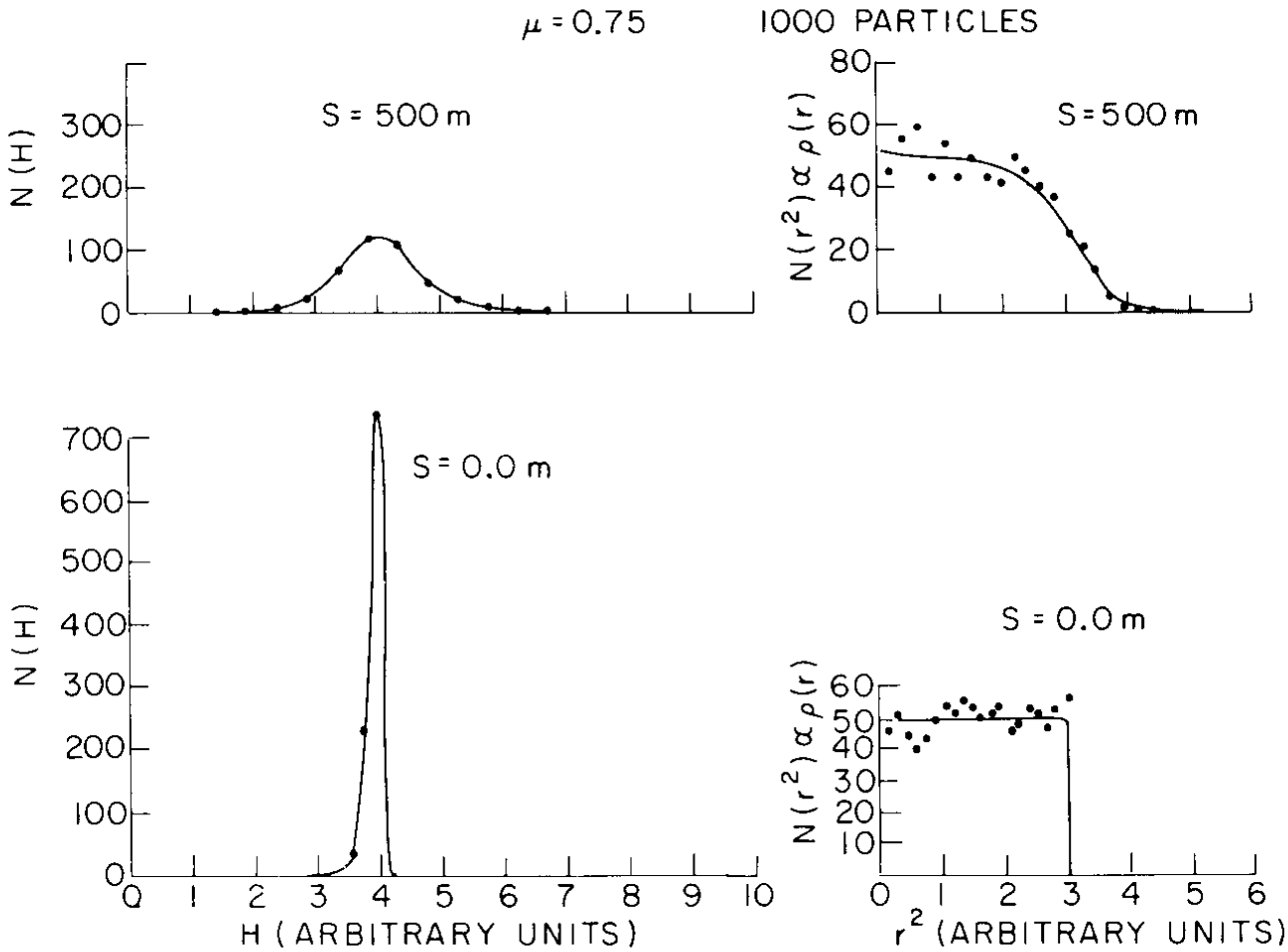

Fig. 13. Distributions in W and radical charge densities at 0 and 500 m, for n = 0 and μ = 0.75, obtained from run with 1000 particles.

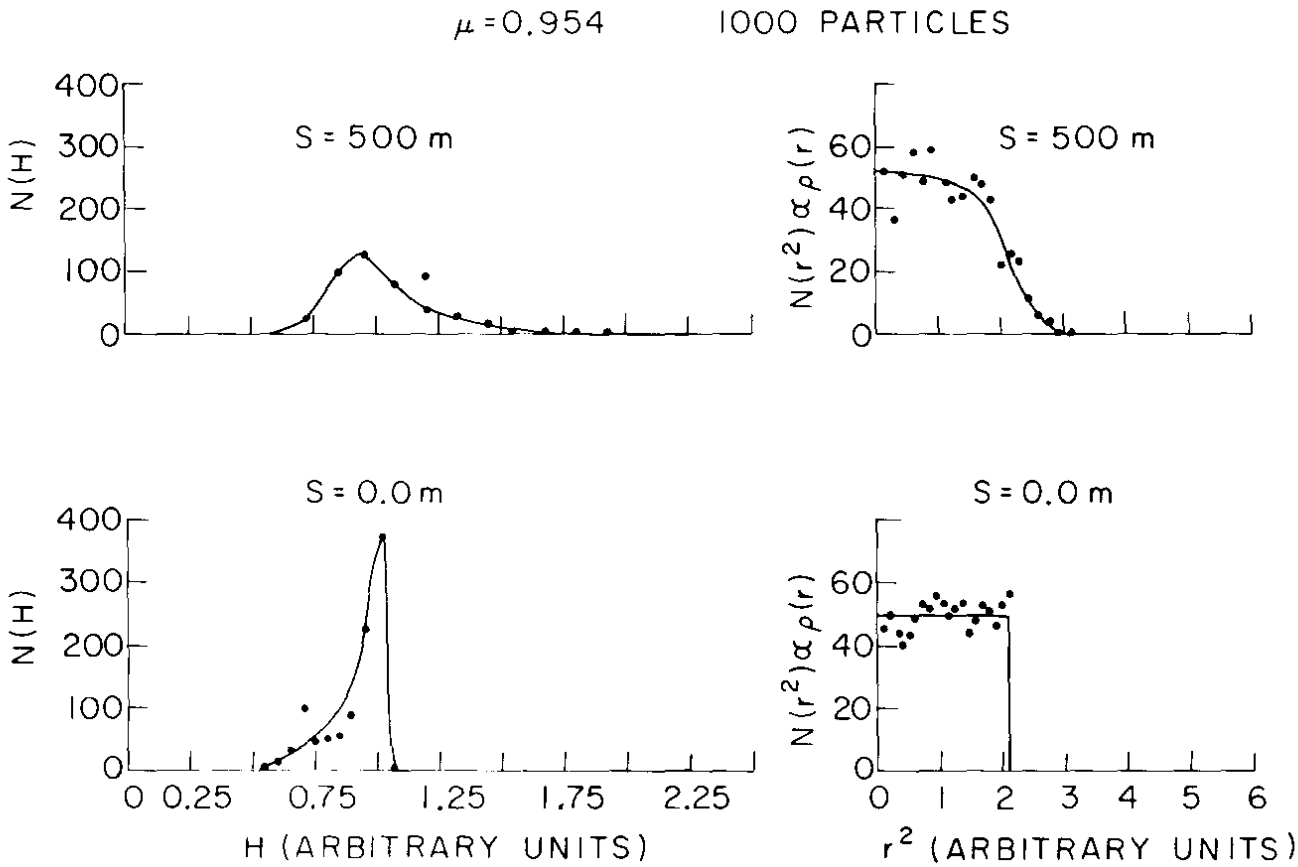

Fig. 14. Distributions in W and radial charge densities at 0 and 500 m, for n = 0 and μ = 0.954, obtained from run with 1000 particles.

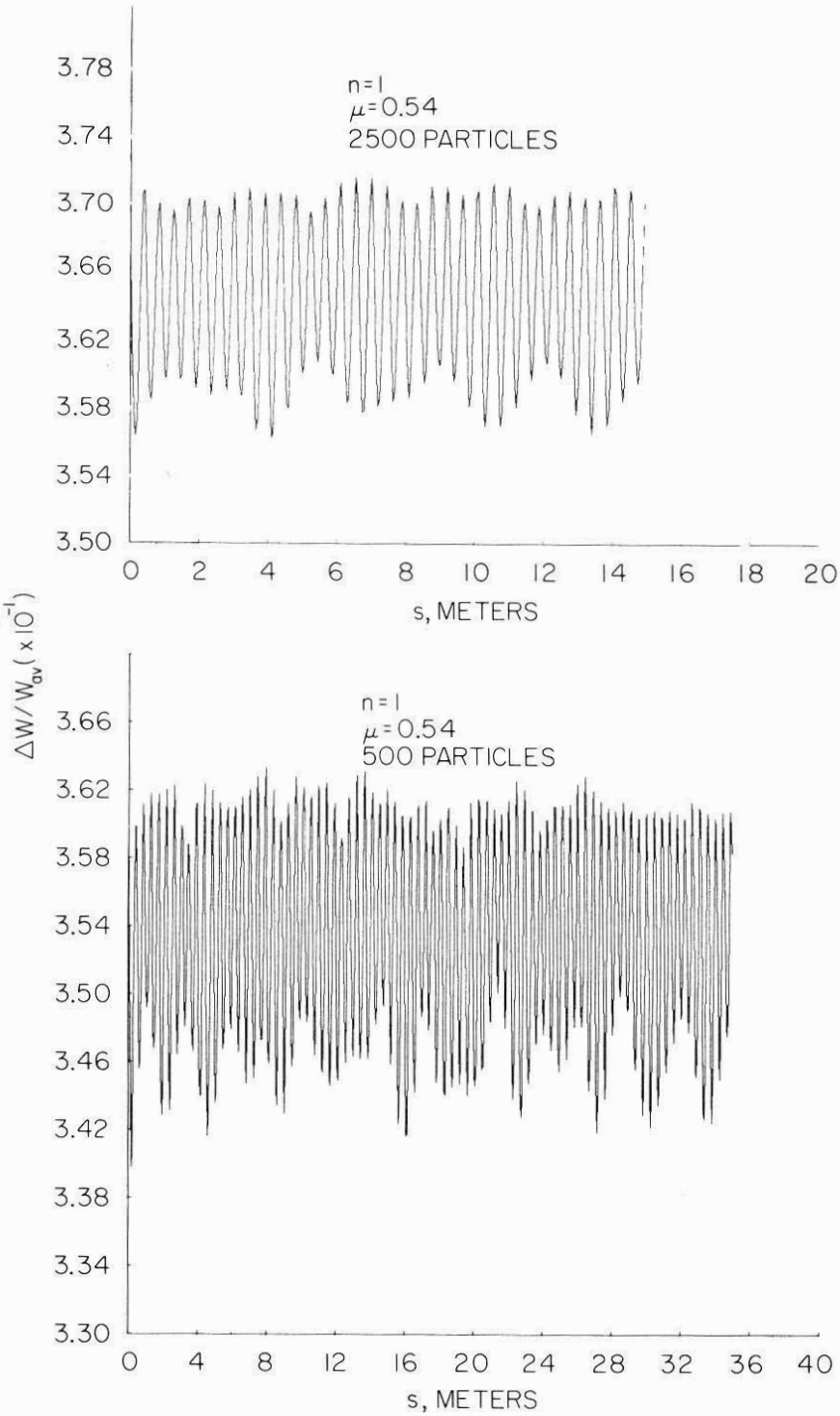

Fig. 15. $\Delta W/W_{av}$ as function of s, for n = 1 and μ = 0.54, obtained from runs with 500 and 2500 particles.

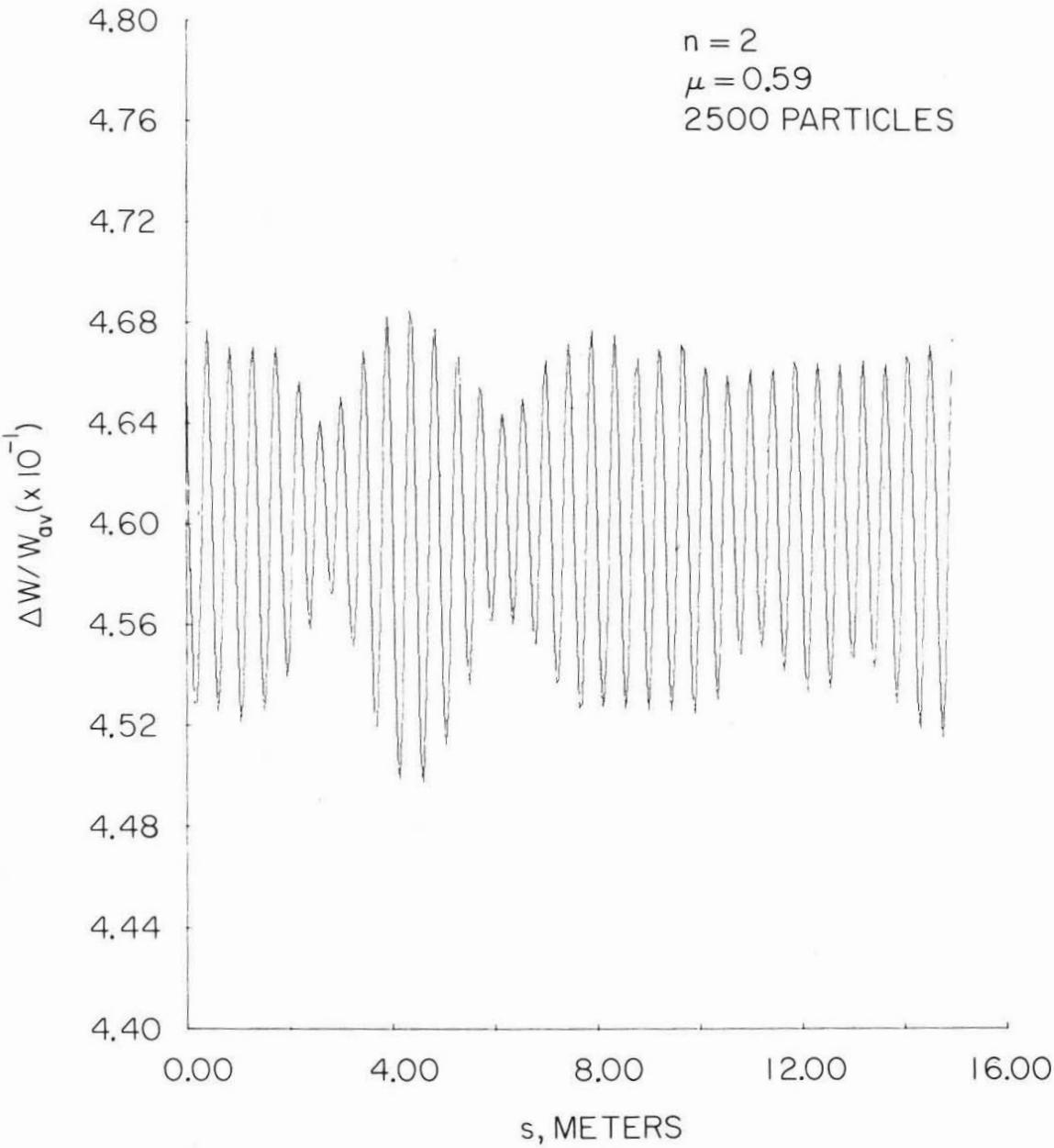

Fig. 16. $\Delta W/W_{av}$ as function of s, for n = 2 and μ = 0.59, obtained from run with 2500 particles.

DISCUSSION

L. C. Teng (NAL): How serious are the higher modes, for example, the (3, 0) and (4, 0) mode?

R. L. Gluckstern (University of Massachusetts): In the higher modes, you find that the synchrotron predictions indicate higher limits. The (2, 0) and the (1, 1) mode are the ones that both indicate the same two-fifths. The higher modes give something much closer to the individual particle frequency. In the case of very high space charge, the (2, 0) mode was the only one which gave an imaginary frequency below $\nu = 1$, so I think it is a serious mode. One should add one comment: this uses the Kapchinski-Vladimirski distribution. If you take some other distribution, then the effort to find these modes is not so easy. We were hoping that the numerical calculations would suggest the form of the modes. Then we could assume a different distribution and try to find these oscillations, their frequencies and parameters of stability. That will be the course of study during the next year or so. The higher modes all involve fluctuations in density in the interior, and they may be more sensitive to the choice of the K-V distribution rather than another one. The lowest mode is an oscillation of the boundary. What we are finding may be correct, but not directly applicable to the real world, because the real distribution will have frequencies and limits that are a little different.

E. Regenstreif (Rennes): In connection with what you have just said, you have used only the K-V distribution, a shell in four-dimensional phase space. We have used a uniform distribution in the xy plane and a Gaussian distribution in velocity space. We found in our numerical calculations that in going 20 cm in accelerating from 50 to 500 keV, we had about three oscillations. But the distribution was uniform at the end in spite of the deformations and distortions. It was a little different from your case, and it would be nice to make a comparison.

R. L. Gluckstern: We have tried other distributions, for example, one uniform in W and one linear in W. Neither showed strong evidence of instability. It is very hard to draw conclusions from the results, even though we have carried the calculations out to hundreds of meters.